Towards an automatic monitoring system of infrasonic events at Mt. Etna: strategies for source location and modelling

P. Montalto
Istituto Nazionale di Geofisica e Vulcanologia, Sezione di Catania, Piazza Roma 2, 95123 Catania, Italy
Dipartimento di Ingegneria Elettrica, Elettronica e dei Sistemi, Università di Catania, Viale Andrea Doria 6, 95125 Catania, Italy

A. Cannata
Istituto Nazionale di Geofisica e Vulcanologia, Sezione di Catania, Piazza Roma 2, 95123 Catania, Italy

E. Privitera
Istituto Nazionale di Geofisica e Vulcanologia, Sezione di Catania, Piazza Roma 2, 95123 Catania, Italy

S. Gresta
Dipartimento di Scienze Geologiche, Università di Catania, Corso Italia 57, 95129 Catania, Italy

G. Nunnari
Dipartimento di Ingegneria Elettrica, Elettronica e dei Sistemi, Università di Catania, Viale Andrea Doria 6, 95125 Catania, Italy

D. Patanè
Istituto Nazionale di Geofisica e Vulcanologia, Sezione di Catania, Piazza Roma 2, 95123 Catania, Italy

Abstract

Active volcanoes characterized by open conduit conditions generate sonic and infrasonic signals, whose investigation provides useful information for both monitoring purposes and studying the dynamics of explosive processes. In this work, we discuss the automatic procedures implemented for a real-time application to the data acquired by a permanent network of five infrasound stations running at Mt. Etna volcano. The infrasound signals at Mt. Etna consist in amplitude transients, called infrasound events. The adopted procedure uses a multi-algorithm approach for event detection, counting, characterization and location. It is designed for an efficient and accurate processing of infrasound records provided by single-site and array stations. Moreover, the source mechanism of these events can be investigated off-line or in near real-time by using three different models: i) Strombolian bubble; ii) resonating conduit and iii) Helmholtz resonator. The infrasound waveforms allow us to choose the most suitable model, to get quantitative information about the source and to follow the time evolution of the source parameters.

Keywords: infrasound, monitoring system, source location, source modelling, Mt. Etna volcano.

1. Introduction

Volcanic unrest is often evidenced by time variations of some physical and geochemical parameters. The geophysical surveillance of volcanoes is routinely performed mainly by observing the patterns of seismic activity and ground deformations (Scarpa and Gasparini, 1996). In recent years, new insights into explosive volcanic processes have been made by studying infrasonic signals (e.g. Vergniolle and Brandeis, 1994; Ripepe et al., 1996; 2001a). Indeed, infrasonic activity on volcanoes is generally evidence of open conduit conditions and can provide important indications on the dynamics of the explosive processes. Unlike the seismic signal, whose wavefield can be strongly affected by topography (Neuberg and Pointer, 2000) and path effects (Gordeev, 1993), the infrasonic signal keeps its features almost unchanged during propagation. In fact, for short distances the infrasonic signal travels in an almost homogenous atmosphere with no structures that can scatter, attenuate or reflect acoustic waves, allowing to easily obtain information on the source. This can be explained by the simpler Green's functions for a fluid atmosphere than those for a complex, heterogeneous volcanic edifice, which supports compressional, shear, and surface waves (Johnson, 2005). However, the source mechanism of the sound radiated during eruptions is still open to debate. Several phenomena are able to generate infrasound signals such as rockfalls or pyroclastic flows (e.g. Moran et al., 2008; Oshima and Maekawa, 2001). Nevertheless, in most cases these signals are related to internal magma dynamics, like the acoustic resonance of fluids in the conduit, triggered by explosive sources; this implies propagation of sound waves in both magma and atmosphere (Garces and McNutt, 1997). According to some authors (e.g. Ferrick et al., 1982; Julian, 1994; Seidl and Hellweg, 2003), seismic and acoustic wave generation in volcanoes can be caused by nonlinear processes. Unlike linear models, nonlinear ones allow the harmonic frequencies to be not proportional to a geometric length scale, which for example may explain why tremor frequencies are similar at volcanoes of vastly different size (Hagerty and Benites, 2003). Another attraction of nonlinear models is that they are able to produce a large range of complex behaviours for relatively small changes in some control parameters (Hagerty and Benites, 2003). Recent studies relate the source of sound to the sudden uncorking of the volcano (Johnson and Lees, 2000), opening of "valves" sealing fluid-filled cracks (Matoza et al., 2009), local coalescence within a magma foam (Vergniolle and Caplan-Auerbach, 2004) and Strombolian bubble vibration (Vergniolle and Brandeis, 1996; Vergniolle et al., 2004). Some techniques have been developed to locate the source of this signal (e.g. Ripepe and Marchetti, 2002; Garces et al., 2003; Johnson, 2005; Matoza et al., 2007; Jones et al., 2008). At multi-vent systems, as Stromboli (Ripepe and Marchetti, 2002), Kilauea (Garces et al., 2003) and Mt. Etna (Cannata et al., 2009a,b), methods based on the comparison of the infrasonic signals by cross correlation or semblance functions have enabled to monitoring and discriminating the explosive activity of distinct craters.

Recently, joint analysis of seismic, infrasonic and thermal signals has proved very useful to investigate explosive processes and distinguish the different eruptive styles and dynamics in various volcanoes, such as Stromboli (Ripepe et al., 2002), Santiaguito (Sahetapy-Engel et al., 2008), Villarica and Fuego (Marchetti et al., 2009). Moreover, recent multiparametric approaches, based on the investigation of infrasound, several different types of seismic signals, such as earthquakes and seismo-volcanic signals, ground deformation and so on, have allowed tracking the evolution of activity in both deep and shallow parts of volcanoes (e.g. Sherrod et al., 2008; Di Grazia et al., 2009; Peltier et al., 2009).

for several years, the surveillance of Mt. Etna volcano (Italy) has been performed by using permanent seismic, GPS, tilt and video camera networks. However, information provided by these networks is sometimes insufficient to characterise well and locate very shallow phenomena such as explosive activity episodes, especially when the visibility of the volcano summit is poor. In the light of this, the staff of Istituto Nazionale di Geofisica e Vulcanologia (INGV) section of Catania has recently started recording and studying the infrasound signal, strictly related to the volcano shallowest dynamics, with the aim of integrating the information provided by the aforementioned networks. During the second half of the 20th century, Mt. Etna was characterized by an unusually high level of eruptive activity, with a clear increase in effusive rates and in the frequency of summit and flank eruptions observed in the last decades (Behncke and Neri, 2003). A remarkable increase in the frequency of short-lived, but violent eruptive episodes at the summit craters has also been observed. Between 1900 and 1970 about 30 paroxysmal eruptive episodes occurred at the summit craters, while there have been more than 180 since then (Behncke and Neri, 2003). The location and characterization of the source of the infrasonic activity are of great importance for the monitoring of the explosive activity of the volcano. The first infrasound investigations at Mt. Etna were performed by temporary experiments (e.g. Ripepe et al., 2001b; Gresta et al., 2004). Since 2006 a permanent infrasound network has been deployed and has allowed to continuously record infrasounds and investigate their link with volcanic activity (Cannata et al., 2009a,b; Di Grazia et al., 2009). The summit area of Mt. Etna is currently characterized by four active craters: Voragine, Bocca Nuova, South-East Crater and North-East Crater (hereafter referred to as VOR, BN, SEC and NEC, respectively; see **Fig. 1**). These craters are characterized by persistent activity that can be of different and sometimes coexistent types: degassing, lava filling or collapses, low rate lava emissions, phreatic, phreato-magmatic or strombolian explosions, and lava fountains (Cannata et al., 2008). Some recent studies have evidenced how the infrasonic signal at Mt. Etna is generally composed of amplitude transients (named infrasonic events), characterised by short duration (from 1 to over 10 s), impulsive compression onsets and peaked spectra with most of energy in the frequency range 1-5 Hz (**Fig. 2;** Gresta et al., 2004; Cannata et al., 2009a,b). Similar features are also observed at several volcanoes, even characterised by different volcanic activity, such as: Stromboli (Ripepe et al., 1996), Klyuchevskoj (Firstov and Kravchenko, 1996), Sangay (Johnson and Lees, 2000), Karymsky (Johnson and Lees, 2000), Erebus (Rowe et al., 2000), Arenal (Hagerty et al., 2000), Tungurahua (Ruiz et al., 2006).

In this paper, we illustrate the architecture of the infrasound monitoring system operating at Mt. Etna, and details of the implemented procedures are also reported. In particular, the techniques of detection and characterization of "infrasonic events", source location and modelling will be described. We will highlight the different features of the events as well as show the importance of the information that the waveform modelling can provide to understand the explosive eruption dynamics.

2. Infrasound monitoring system

Infrasound at Mt. Etna has been routinely monitored from September 2006. The permanent infrasound network of Mt. Etna, run by INGV, Section of Catania, comprises five stations, located at distances ranging between 1.5 and 7 km from the centre of the summit area (**Fig. 1**). The whole system may be described by the following parts: i) data acquisition, ii) event detection, iii) event

characterization, iv) source location and v) modelling (**Fig. 3**). The steps i-iv) are designed for a real-time application, whereas the step v) for near real-time or off-line analysis.
The most active vents during 2007-2008 were SEC and NEC, mainly characterised by explosive and degassing activity, respectively. Moreover, an eruptive fissure (EF in **Fig. 1**) opened on May 13, 2008, in the upper part of the Valle del Bove and was characterised by both effusive and explosive activity, ended on July 6, 2009.

2.1 Data acquisition

The infrasonic sensors consist of a Monacor condenser microphone MC-2005, with a sensitivity of 80 mV/Pa in the 1–20 Hz infrasonic band. The infrasonic signals are transmitted in real-time by radio link to the data acquisition centre in Catania where they are acquired at a sampling rate of 100 Hz.

2.2 Event detection

Once the infrasound signal is recorded, the signal portions of interest, which are the infrasonic events, have to be extracted. A reference station is chosen, according to the best signal to noise ratio. At Mt. Etna we use EBEL as reference station. Therefore, the STA/LTA (short time average/long time average) method is applied, that evaluates the ratio of short- to long-term energy density. The optimal window lengths of STA and LTA depend on the frequency content of the investigated signal (e.g. Withers et al., 1998). This method is used both to pick the onset of the events and to count them. The picking allows performing the location analysis (see **section 2.4**). The rate of occurrence of infrasonic events is useful for monitoring explosive activity. In fact, the occurrence rate of the events increases during the explosive activity (see **Fig. 4**). The efficiency of videocameras and thermal sensors, that visually detect changes in explosive activity (Bertagnini et al., 1999; Harris et al., 1997), is strongly reduced (or inhibited) if there are clouds, fog or gas plumes. Thus the detection and characterization of explosive activity by infrasounds is very useful especially when the visibility of the volcano summit is poor (e.g. Cannata et al., 2009a).
Nevertheless, it is worth noting that infrasonic events occurring during lava fountains are not detectable. The very high occurrence rate of events during the paroxysmal stages gives rise to an almost continuous signal (the so-called infrasonic tremor), preventing the detection of single events. On the other hand, also the events occurring during periods characterised by strong wind are not detectable because of the high noise.

2.3 Event characterization

Recent studies performed at Mt. Etna have allowed recognising SEC and NEC as the most active summit craters from an infrasonic point of view (Cannata et al., 2009a,b). During 2007-2008 the former was characterised by both degassing and explosive activity (strombolian activity and lava fountaining), while the latter mainly by degassing. According to Cannata et al. (2009a,b) these craters generate infrasound signals with different spectral features and duration: “NEC events”, lasting up to 10 seconds and characterised by dominant frequency generally lower than 2.5 Hz, are related to the degassing activity of NEC and are recorded almost continuously (**Fig. 2a**); “SEC events”, with duration of about 2 seconds, dominant frequency mainly higher than 2.5 Hz and higher peak-to-peak amplitude than the NEC events, are recorded during explosive activity at SEC (**Fig. 2b**). Moreover, during the 2008-2009 eruption a third infrasound source, coinciding with the lowermost tip of the eruptive fissure, was active. During periods with explosive activity, this source generated signals, called “EF events”, with features similar to the SEC events (**Fig. 2c**).

On this basis and according to Cannata et al. (2009b), a simple spectral analysis of the infrasonic events recorded at a single station, together with the amplitude estimation, can give preliminary information on the ongoing volcanic activity and active craters. In particular, spectral and amplitude variations over time of such infrasound signals can be a good indicator of changes in the volcanic activity. Therefore, the third step of the automatic monitoring system consists of extracting spectral features and the peak-to-peak amplitudes from the waveforms of the detected events (**Fig. 3**). As shown in Cannata et al. (2009b), Sompi method (Kumagai, 2006 and reference therein) is a useful algorithm to calculate the dominant frequency and the quality factor of the events. Similarly to the detecting step, the infrasound characterization is carried out on the signal recorded by EBEL, considered as reference station.

In **Fig. 5** the time variation of peak-to-peak amplitude, frequency and quality factor values of events, recorded during January-June 2008, is reported, together with the source location and a scheme summarising the volcanic activity. There are strict relationships between variations of the infrasound event features and changes in the eruptive activity (**Fig. 5**). For example the explosive activity at SEC, taking place on February 12, 2008, and mainly consisting in ash emission (Corsaro, 2008), was accompanied by increases in both amplitudes and frequency peak values. Similar changes in the infrasound activity occurred on May 13, 2008, at the onset of the eruption at the eruptive fissure opened on the same day in the upper part of the Valle del Bove (Di Grazia et al., 2009).

2.4 Source location

Unlike the seismic source location, whose epicentral location resolution is seldom better than 100 m, the infrasonic location can be as good as 3 m for a well-positioned array (Johnson, 2005). This difference is due to the much lower propagation velocity of the infrasonic waves (roughly 340 m/s) than the seismic ones (generally >1000 m/s).

Different techniques have been developed to locate the infrasound sources (e.g. Ripepe and Marchetti, 2002; Garces et al., 2003; Johnson, 2005; Matoza et al., 2007; Jones et al., 2008). At Mt. Etna, the location is performed by using the semblance method (Neidell and Taner, 1971), which is also followed to locate long period (LP) and very long period (VLP) events at the same volcano (e.g. Patanè et al., 2008; Cannata et al., 2009c). This method is based on the semblance function that is a measure of the similarity of multichannel data. Considering traces *U* acquired by a certain number of sensors *N*, the semblance is defined as (Neidell and Taner, 1971):

$$S_0 = \frac{\sum_{j=1}^{M}\left(\sum_{i=1}^{N} U_i(\tau_i + j\Delta t)\right)^2}{N\sum_{j=1}^{M}\sum_{i=1}^{N} U_i(\tau_i + j\Delta t)^2} \tag{1}$$

where Δt is the sampling interval, τ_i is the origin time of the window sampling the *i*-th trace, $U_i(\tau_i + j\Delta t)$ is the *j*-th time sample of the trace *i*-th *U*, and *M* represents the number of samples in the window. S_0 is a number between 0 and 1. The value 1 is only reached when the signals are identical, not only in waveform but also in amplitude. If the traces are normalized, and then the semblance values only depend on the shape of the signals, it can be demonstrated that the definition of semblance is equivalent to an averaging of the correlation coefficients of all the possible trace pairs (Almendros and Chouet, 2003). The semblance method consists in finding a set of arrival times (τ_i, $i = 1,\ldots, N$), that yields a maximum semblance for the *N*-channel data. The procedure is composed of several steps. First of all, a broad enough region of interest has to be determined to include the actual source. Since the vent radiating infrasound can be considered a source point located on the topographical surface, this region can be defined by bi-dimensional grid of assumed source positions coinciding with the topography. A start time t_s is fixed as the time of first arrival at a reference station (generally chosen on the basis of the highest signal to noise ratio) by visual inspection or triggering algorithm (see **section 2.2**). The source is assumed to be in each node of the grid, and for each node the origin time t_o is calculated, assuming a certain value of propagation velocity of the infrasonic waves *v* (generally considered equal to 340 m/s; Lighthill, 1978), as follows:

$$t_o = t_s - r/v \quad (2)$$

where r is the distance between the reference station and the node of the grid assumed as source location. Successively, the theoretical travel times are calculated at all the sensors t_i (i = 1,…, N, number of stations):

$$t_i = r_i/v \quad (3)$$

where r_i is the distance between the station i-th and the node of the grid assumed as source location. Then, by these theoretical travel times and the origin time, signals at the different stations are delayed and compared by the semblance function. Signal windows containing between one and two cycles of the dominant period are generally used to calculate the semblance value because they provide the best performance (Almendros and Chouet, 2003). Therefore, the semblance function is assumed representative of the probability that a node has to be the source location. The source is finally located in the node where the delayed signals show the largest semblance value. This method is suited to locate infrasound events recorded by sensors arranged in sparse networks as well as with array configurations.

Since the location procedure is to be performed in near real-time, the computational time has to be shorter than the analysed period. Therefore, if the event rate is high and then not all the detected events can be located, only the "best" transients must be analysed. The choice is based on both the signal to noise ratio at all the available stations and the peak-to-peak amplitude of the events at the reference station. Finally, the number of events that can be located depends on the used space grid and on the available computational power.

We locate the infrasonic source by the permanent network of **Fig. 1** by using a grid of 2.5×2.5 km, with spacing of 10 m. For example during 2007-2008 three different sources, coinciding with NEC, SEC and EF have been found. In **Fig. 6** three examples of semblance distribution and infrasound traces are reported. It is worth noting that, as infrasonic signals are sinusoidal, semblance space distribution is roughly sinusoidal too. The wavelength of such sinusoidal semblance function strictly depends on the wavelength of the infrasonic event. The higher the frequency of the infrasound event, the shorter the wavelength of the semblance function. **Fig. 5** and **7** show the source locations of some events detected during January-June 2008.

In order to estimate the location error, the method described in Almendros and Chouet (2003) and applied on VLP events can be followed by simply replacing the seismic signals with the infrasound ones and considering a 2D rather than a 3D space distribution of semblance values. Firstly, we calculate the signal to noise ratio (hereafter called *SNR*) for the event by the following equation (derived from the equation 15 in Almendros and Chouet, 2003):

$$SNR = \frac{1}{N}\sum_{i=1}^{N}\frac{\sigma_i^s - \sigma_i^n}{\sigma_i^n} \tag{4}$$

where N is the number of stations, σ_i^s and σ_i^n are RMS (root mean square) of the infrasound signal windows at the i-th station containing the event and only noise preceding the event, respectively. σ_i^s and σ_i^n are obtained taking into account 2-second-long and 10-second-long windows, respectively. Successively, in order to define an error region, a semblance threshold, indicated by S_{th}, is fixed for each event such that:

$$S_{th} = (1 - \delta S)\, S_{max} \tag{5}$$

where S_{max} is the maximum value of semblance, reached in the whole grid, and δS, depending on *SNR* value, is given by (equation 16 in Almendros and Chouet, 2003):

$$\delta S = 0.062\, SNR^{-1.54} \tag{6}$$

Finally, the extension of the region with semblance value higher than S_{th} is calculated in the two space directions (longitude and latitude) and the corresponding errors are estimated (see error bar in **Fig. 5e,f**).

2.5 Source modelling

Following the sketch of **Fig. 3**, once the waveforms of infrasonic events have been extracted and characterized, and the source located, the source mechanism can be investigated. Since this task is not critical from the monitoring point of view, it can be performed in near real-time or even off-line. As aforementioned the source process of infrasound in volcanic areas is still open to debate. However, among the infrasound source models (mentioned in **section 1)**, three have been well developed and applied on observed data: 1) the resonating conduit (Buckingham and Garces, 1996; Garces and McNutt, 1997; Hagerty et al., 2000); 2) the Strombolian bubble vibration (Vergniolle and Brandeis, 1994, 1996; Vergniolle et al., 1996, 2004; Vergniolle and Ripepe, 2008); 3) the local coalescence within a magma foam (Vergniolle and Caplan-Auerbach, 2004).

The first model is based on a pipe-like conduit, that, if affected by trigger mechanisms such as explosive processes, can resonate generating seismic and infrasonic signals, whose waveforms strictly depend on the geometrical-chemical-physical features and specific boundary conditions of the conduit (see **Appendix A1**). The acoustic signal, thus generated, consists in gradually decaying sinusoids with a fundamental mode and harmonics. A candidate example recorded at Mt. Etna is shown in **Fig. 2a**.

On the other hand, in the Strombolian bubble vibration model the infrasound is produced by the vibration of a thin layer of magma, pushed by a variation of pressure inside a shallow metric bubble prior to bursting (see **Appendix A2**). The bubble shape is approximated by a hemispherical head and a cylindrical tail, as expected in slug-flow (**Fig. 8a**). The propagation of pressure waves is radial and the waveform of the resulting infrasound signal is composed of a first energetic part roughly composed of one cycle – one cycle and a half (corresponding to the bubble vibration), followed by a second part with various weaker oscillations sometimes with higher frequency (radiated during and after the bubble bursting) (e.g. **Fig. 2b,c**).

Finally, according to the Helmholtz resonator model the source of infrasound signals is the coalescence of the very shallow part of a foam building up into the conduit, which produces large gas bubbles (see **Appendix A3**). In this case the gas escapes through a tiny upper hole. The shape of the bubble is similar to the Strombolian bubble model with the exception of a tiny upper hole (**Fig. 8b**). The resulting acoustic signal consists in gradually decaying monochromatic sinusoids and can be modelled by a Helmholtz resonator (Vergniolle and Caplan-Auerbach, 2004). Also this source mechanism, like the resonating conduit model, could give rise to harmonics in the signal. In fact the event in **Fig. 2a** can be interpreted as generated either by a resonating conduit or by a Helmholtz resonator.

The infrasound events at Mt. Etna, recorded during 2007-2008, can be interpreted as generated by the aforementioned source models.

The choice of the model to apply strictly depends on the waveform of the investigated signal. If the infrasound signal is composed of one cycle – one cycle and a half, followed by a second part with weaker oscillations (**Fig. 2b,c**), the Strombolian bubble model should be applied. On the other hand, if the infrasonic event is characterized by gradually decaying sinusoids with a fundamental mode and harmonics or with monochromatic spectral content (**Fig. 2a**), two different models can be applied: the resonating conduit and the Helmholtz resonator. The method to choose the model has still to be defined. We suggest using the damping features of the oscillations composing the infrasonic events as a quantitative parameter indicating the source type. For example, slow damping, that means many cycles, would be indicative either of a resonating conduit or of a Helmholtz resonator. Conversely, quick damping, and then one or two cycles, could be due to a Strombolian bubble model. Therefore, the quality factor values, computed in the iii) step and describing the damping features of the infrasound waveforms, can be chosen as a model discriminator. If the quality factor is less than a certain threshold the Strombolian bubble model will be applied, otherwise the Helmholtz resonator or the resonating conduit model will be considered.

In the resonating conduit model, if there is information about the fluid filling the conduit, the length of the resonating portion of the conduit can be calculated by using the **equation (A1)**. For example assuming that the event, shown in **Fig. 2a** and generated by the NEC, is caused by a resonant conduit and that the fluid filling the conduit is gas, we infer that the length of the resonating portion of the conduit roughly ranges between 150 and 320 m, according to the air/gas conditions. However, since the ranges of variability of fluid features are very wide and the conduit resonance model oversimplified, the variations over time of the model parameters are to be taken into account rather than the exact values. In the other two models, there are three unknown source parameters: radius of the bubble/hole (Strombolian bubble and Helmholtz resonator models, respectively), length of the bubble and initial overpressure (R or R_{hole}, L and ΔP, respectively). It is worth noting that the Helmholtz resonator model requires that the radius of the bubble, which can be inferred by the vent radius, is known. In order to constrain these unknowns, the estimation of the similarity between synthetic and observed infrasound signals is required. The synthetic signals can be calculated by using the **equations (A12)** and **(A13)** for the Strombolian bubble and Helmholtz resonator models, respectively. The comparison is carried out by the following equation:

$$E = \frac{\sum_{i=1}^{M} \left(U_{obs\ i} - U_{syn\ i} \right)^2}{M} \tag{7}$$

where E is the misfit between observed and synthetic signals, called prediction error, U_{obs} and U_{syn} are the observed and synthetic signals, and M is their number of samples.

Model identification consists of two tasks. The first task is a structural identification of the equations and the second one is an estimation of the model parameters. The optimization method chosen to look for the best fit between observed and synthetic signals is the Genetic Algorithm (GA) that applies Darwin's evolutionary theory to general optimization problems. This kind of algorithm represents a highly idealized model of a natural process and as such can be legitimately viewed as a very high level of abstraction. Biological strategies of behaviour adaptation and synthesis are used to enhance the probability of survival and propagation during their evolution (Ghoshray et al., 1995). This method is based on individuals*,* grouped into populations that represent the parameters searched in the estimation process. The GA method can be reassumed by the following steps: i) an initial set of candidate solutions, called initial population, are generated; ii) the evaluation of the candidate solutions is performed according to some fitness criteria; iii) on the basis of the performed evaluation some candidate solutions are kept and the others are discarded; iv) finally, certain variants are produced by using some kinds of operator on the surviving candidate solutions (Mitchell, 1996). The identification problem can be formulated as an optimization task whose aim is to find a set of parameters that minimize the prediction error between measured data and the model output (**Fig. 9**). The inversion task can be considered completed if the prediction error is lower than a fixed threshold or if a time-out condition occurs. In the former case the source parameters are stored in a database, while in the latter the event is discarded (**Fig. 9**).

Following Vergniolle and Caplan-Auerbach (2004), when the Helmholtz resonator model is applied, the fit between observed and synthetic signals should be optimised at the beginning of the oscillations in case there are other sources of damping not considered in the model. Examples of waveform inversion are reported in **Fig. 10**. By the waveform inversion of the event of **Fig. 10a**, due to Strombolian bubble vibration, the obtained radius and length of the bubble were equal to 4 m and 6 m, respectively, with an initial overpressure of 0.13 MPa. On the other hand, assuming that the event reported in **Fig. 10b** was generated by the Helmholtz resonator and fixing the bubble radius to 6 m, the obtained radius of the hole and length of the bubble would be equal to 0.5 m and 40 m, respectively, with an initial overpressure of 0.02 MPa. Similarly to the resonating conduit model, also the changes over time of the calculated source parameters of Helmholtz resonator and Strombolian bubble models can be important information to track the evolution of the volcanic activity. Vergniolle and Ripepe (2008), studying the infrasound signals during the explosive activity occurring at Mt. Etna on July 12, 2001, noted bubble length increases at the transition towards lava fountain.

3. Conclusions

During recent decades global infrasound monitoring systems have been developed to provide notification and information about energetic events taking place in the atmosphere, such as bolides, rocket launches, explosions and lightning (e.g. Hedlin et al., 2002; Arrowsmith et al., 2008; Assink et al., 2008). These systems have also proved very useful to remotely detect volcanic eruptions (e.g. Evers and Haak, 2005; Guilbert et al., 2005). However, detailed and precise data regarding location of the active vents and infrasound source mechanism require dedicated infrasonic observations close to volcanoes (e.g. Ripepe and Marchetti, 2002; Vergniolle and Ripepe, 2008; Cannata et al., 2009a,b). This information is very useful for the monitoring of explosive activity (e.g. Ripepe et al., 2001a; Johnson, 2005; Cannata et al., 2009a) and to shed a light on explosive eruption dynamics. To this end, we have developed an infrasound monitoring system at Mt. Etna (**Fig. 3**). First of all, it allows extracting the signal portions of interest and to investigate time variations of the occurrence rate of the infrasonic events. Then, preliminary information on the ongoing volcanic activity and active craters can be provided by the investigation of the infrasonic waveforms in terms of peak-to-peak amplitude and spectral features. Successively, an effective location method, based on the similarity of multi-channel data, enables pinpointing the vent generating acoustic waves. Finally, in order to investigate the source mechanisms and the related parameters the source modelling is performed. Unlike the previous steps of this system that are designed as real-time applications, the source modelling, considered a non-critical task from a monitoring point of view, is developed as near real-time or even off-line analysis. Three infrasound source models are explained in detail highlighting the main features of the generated infrasound signals as well as the main information provided. In particular, by constraining bubble radius, length and overpressure, the bubble volume can be computed for both Strombolian bubble and Helmholtz resonator models. Then, the gas volume expelled in the atmosphere can be deduced from the bubble volume at the vent by using the overpressure values and the perfect gas law (Vergniolle and Ripepe, 2008). By summing the gas volume obtained for all the infrasonic events, the degassing rate of the volcano can also be estimated (Cannata et al., 2009b). However, since gas at volcanoes is also emitted without detectable infrasound radiation (Vergniolle and Ripepe, 2008), the estimated gas flux is to be considered an underestimation. Finally, the bubble radius can be considered as an estimation of the vent radius, while the overpressure as a useful parameter to estimate the "strength of an eruption" (Vergniolle et al., 2004).

Summing up, infrasound signal analyses enable us to obtain useful information on the volcanic activity, on its location and on the characteristics of the acoustic source. The described automatic monitoring system represents a step forward in our ability to monitor and understand volcanic phenomena. The next step will be the development of an integrated multiparametric system. This should be able to collect information provided by automatically analysing not only infrasound events but also seismo-volcanic signals, such as volcanic tremor, LP and VLP signals.

Acknowledgements

We thank an anonymous reviewer for her/his constructive suggestions that helped us to significantly improve our manuscript. Work partly performed in the framework of the DPC-INGV (2007-2009) Project.

References

Aki, K., Fehler, M., and Das, S. (1977), *Source mechanism of volcanic tremors: fluid driven crack models and their application to the 1963 Kilauea eruption*, J. Volcanol. Geotherm. Res. *2*, 259–287.

Almendros, J., and Chouet, B. (2003), *Performance of the radial semblance method for the location of very long period volcanic signals*, Bull. Seismol. Soc. Am. *93*, 1890-1903.

Arrowsmith, S., ReVelle, D., Edwards, W., and Brown, P. (2008), *Global detection of infrasonic signals from three large bolides*, Earth Moon Planet *102*, 357-363.

Assink, J.D., Evers, L.G., Holleman, I., and Paulssen, H. (2008), Characterization of infrasound from lightning, *Geophys. Res. Lett. 35*, L15802, doi:10.1029/2008GL034193.

Behncke, B. and Neri, M. (2003), *Cycles and trends in the recent eruptive behaviour of Mount Etna (Italy)*, Can. J. Earth Sci. *40*, 1405-1411.

Bertagnini, A., Coltelli, M., Landi, P., Pompilio, M., and Rosi, M. (1999), *Violent explosions yield new insights into dynamics of Stromboli volcano*, EOS *80*, 633– 636.

Buckingham, M.J., and Garces, M.A. (1996), *A canonical model of volcano acoustics*, J. Geophys. Res. *101*, 8129-8151.

Cannata, A., Catania, A., Alparone, S., and Gresta, S. (2008), *Volcanic tremor at Mt. Etna: Inferences on magma dynamics during effusive and explosive activity*, J. Volcanol. Geotherm. Res. doi:10.1016/j.jvolgeores.2007.11.027.

Cannata, A., Montalto, P., Privitera, E., Russo, G., and Gresta, S. (2009a), *Tracking eruptive phenomena by infrasound: May 13, 2008 eruption at Mt. Etna*, Geophys. Res. Lett. doi:10.1029/2008GL036738.

Cannata, A., Montalto, P., Privitera, E., and Russo, G. (2009b), *Characterization and location of infrasonic sources in active volcanoes: Mt. Etna, September-November 2007*, J. Geophys. Res. *114*, B08308, doi:10.1029/2008JB006007.

Cannata, A., Hellweg, M., Di Grazia, G., Ford, S., Alparone, S., Gresta, S., Montalto, P., and Patanè, D. (2009c), *Long Period and Very Long Period events at Mt. Etna volcano: characteristics, variability and causality, and implications for their sources*. J. Volcanol. Geothherm. Res., doi: 10.1016/j.jvolgeores.2009.09.007.

Corsaro, R.A. (2008), *Rapporto settimanale sull'attività eruttiva dell'Etna (11 – 17 febbraio 2008)* (in Italian), volcanological report, Ist. Naz. di Geofis. e Vulcanol., Catania, Italy, (Available at http://www.ct.ingv.it/Report/WKRVGREP20080217.pdf)

De Angelis, S., and McNutt, S.R. (2007), *Observations of volcanic tremor during the January–February 2005 eruption of Mt. Veniaminof, Alaska,* Bull. Volcanol. *69*, 927-940.

Di Grazia, G., Cannata, A., Montalto, P., Patanè, D., Privitera, E., Zuccarello, L., and Boschi, E. (2009), *A new approach to volcano monitoring based on 4D analyses of seismo-volcanic and acoustic signals: the 2008 Mt. Etna eruption*, Geophys. Res. Lett. *36*, L18307, doi:10.1029/2009GL039567.

Evers, L.G., and Haak, H.W. (2005), *The detectability of infrasound in The Netherlands from the Italian volcano Mt. Etna*, J. Atmosph. Sol. Terr. Phys. *67*, 259-268.

Ferrick, M.G., Qamar, A., and Lawrence, W.F. (1982), *Source mechanism of volcanic tremor*, J. Geophys. Res. *87* (B10), 8675-8683.

Firstov, P.P., and Kravchenko, N.M. (1996), *Estimation of the amount of explosive gas released in volcanic eruptions using air waves*, Volcanol. Seismol. *17*, 547-560.

Garces, M.A., and McNutt, S.R. (1997), *Theory of the airborne sound field generated in a resonant magma conduit*, J. Volcanol. Geotherm. Res. *78*, 155-178.

Garces, M., Harris, A., Hetzer, C., Johnson, J., Rowland, S., Marchetti, E., and Okubo, P. (2003), *Infrasonic tremor observed at Kilauea Volcano, Hawaii*, Geophys. Res. Lett. *30*, 2023, doi:10.1029/2003GL018038.

Ghoshray, S., and Yen, K.K. (1995), *More efficient genetic algorithm for solving optimization problems.* Proceedings of the 1995 IEEE International Conference on Systems for the 21st Century, 4515–4520.

Gordeev, E.I. (1993), *Modelling of volcanic tremor as explosive point sources in a singled-layer, elastic half-space*, J. Geophys. Res. *98*, 19687-19703.

Gresta, S., Ripepe, M., Marchetti, E., D'Amico, S., Coltelli, M., Harris, A.J.L., and Privitera, E. (2004), *Seismoacoustic measurements during the July-August 2001 eruption at Mt. Etna volcano, Italy*, J. Volcanol. Geotherm. Res. *137*, 219-230.

Guilbert, J., Harjadi, P., Purbawinata, M., Jammes, S., Le Pichon, A., and Feignier, B. (2005), *Monitoring of Indonesian volcanoes with infrasound: preliminary results*, 2005 Infrasound Technology Workshop, Tahiti.

Hagerty, M.T., Schwartz, S.Y., Garces, M.A., and Protti, M. (2000), *Analysis of seismic and acoustic observations at Arenal Volcano, Costa Rica, 1995-1997*, J. Volcanol. Geotherm. Res. *101*, 27-65.

Hagerty, M., and Benites, R. (2003), *Tornillos beneath Tongariro Volcano, New Zealand*, J. Volcanol. Geotherm. Res. *125* doi: 10.1016/S0377-0273(03)00094-5.

Harris, A.J.L., Blake, S., Rothery, D.A., and Stevens, N.F. (1997), *A chronology of the 1991 to 1993 Mount Etna eruption using advanced very high resolution radiometer data: Implications for real-time thermal volcano monitoring*, J. Geophys. Res. *102*, 7985–8003.

Hedlin, M.A.H., Garces, M., Bass, H., Hayward, C., Herrin, G., Olson, J., and Wilson, C. (2002), *Listening to the secret sounds of Earth's atmosphere*, EOS *83*, 564–565.

Johnson, J.B., and Lees, J.M. (2000), *Plugs and chugs: seismic and acoustic observations of degassing explosions at Karymsky, Russia and Sangay, Ecuador*, J. Volcanol. Geotherm. Res. *101*, 67-82.

Johnson, J.B. (2005), *Source location variability and volcanic vent mapping with a small-aperture infrasound array at Stromboli Volcano, Italy*, Bull. Volcanol. *67*, 1-14.

Jones, K.R., Johnson, J., Aster, R., Kyle, P.R., and McIntosh, W.C. (2008), *Infrasonic tracking of large bubble bursts and ash venting at Erebus volcano, Antarctica*, J. Volcanol. Geotherm. Res., doi: 10.1016/j.jvolgeores.2008.02.001.

Julian, B.R. (1994), *Volcanic tremor: nonlinear excitation by fluid flow*, J. Geophys. Res. *99* (B6), 11859-11877.

Kumagai, H. (2006), *Temporal evolution of a magmatic dike system inferred from the complex frequencies of very long period seismic signals*, J. Geophys. Res. *111*, B06201. doi:10.1029/2005JB003881.

Lighthill, J. (1978), *Waves in Fluids*, Cambridge University Press. 504 pp.

Matoza, R.S., Hedlin, M., and Garces, M. (2007), *An infrasound array study of Mount St. Helens*, J. Volcanol. Geotherm. Res. *160*, 249-262.

Matoza, R.S., Garces, M.A., Chouet, B., D'Auria, L., Hedlin, H., De Grooth-Hedlin, C., and Waite, G.P. (2009), *The source of infrasound associated with long-period events at Mount St. Helens*, J. Geophys. Res. *114*, doi:10.1029/2008JB006128.

Mitchell, M. (1996), *An Introduction to Genetic Algorithms*, MIT Press, Cambridge, 205 pp.

Moran, S.C., Matoza, R.S., Garces, M.A., Hedlin, H., Bowers, D., Scott, W.E., Sherrod, D.R., and Vallance, J.W. (2008), *Seismic and acoustic recordings of an unusually large rockfall at Mount St. Helens, Washington*, Geophys. Res. Lett. *35*, doi:10.1029/2008GL035176.

Murase, T., and McBirney, A.R. (1973), *Properties of some common igneous rocks and their melts at high temperatures*, Geol. Soc. Am. Bull. *84*, 3563-3592.

Neidell, N., and Taner, M.T. (1971), Semblance and other coherency measures for multichannel data, Geophysics *36*, 482-497.

Neuberg, J., and Pointer, T. (2000), Effects of volcano-topography on seismic broadband waveforms, Geophys. J. Int. *143*, 239-248.

Oshima, H., and Maekawa, T. (2001), *Excitation process of infrasonic waves associated with Merapi-type pyroclastic flow as revealed by a new recording system*, Geophys. Res. Lett. *28*, 1099-1102.

Patanè, D., Di Grazia, G., Cannata, A., Montalto, P., and Boschi, E. (2008), *The shallow magma pathway geometry at Mt. Etna volcano*, Geochem. Geophys. Geosyst. *9*, doi:10.1029/2008GC002131.

Peltier, A., Bachèlery, P., and Staudacher, T. (2009), *Magma transport and storage at Piton de La Fournaise (La Réunion) between 1972 and 2007: A review of geophysical and geochemical data*. J. Volcanol. Geotherm. Res. *148*, 93-108.

Ripepe, M., Poggi, P., Braun, T., and Gordeev, E. (1996), Infrasonic *waves and volcanic tremor at Stromboli*, Geophys. Res. Lett. *23*, 181-184.

Ripepe, M., Ciliberto, S., and Della Schiava, M. (2001a), *Time constraint for modelling source dynamics of volcanic explosions at Stromboli*, J. Geophys. Res. *106*, 8713-8727.

Ripepe, M., Coltelli, M., Privitera, E., Gresta, S., Moretti, M., and Piccinini, D. (2001b), *Seismic and infrasonic evidences for an impulsive source of the shallow volcanic tremor at Mt. Etna, Italy*, Geophys. Res. Lett. *28*, 1071-1074.

Ripepe, M., and Marchetti, E. (2002), Array tracking of infrasonic sources at Stromboli volcano, Geophys. Res. Lett. *29*, 2076, doi:10.1029/2002GL015452.

Rowe, C.A., Aster, R.C., Kyle, P.R., Dibble, R.R., and Schlue, J.W. (2000), *Seismic and acoustic observations at Mount Erebus Volcano, Ross Island, Antarctica, 1994-1998*, J. Volcanol. Geotherm. Res. *101*, 105-128.

Ruiz, M.C., Lees, J.M., and Johnson, J.B. (2006), *Source constraints of Tungurahua volcano explosion events*, Bull. Volcanol. *68*, 480-490.

Scarpa, R., and Gasparini, P. (1996), *A review of volcano geophysics and volcano-monitoring methods*. In *Monitoring and mitigation of volcano hazards* (eds. Scarpa, Tilling), pp. 3-22.

Seidl, D., and Hellweg, M. (2003), *Parameterization of multichromatic tornillo signals observed at Galeras Volcano (Colombia)*, J. Volcanol. Geotherm. Res. *125*, 171-189.

Sherrod, D.R., Scott, W.E., and Stauffer, P.H. (2008), *A volcano rekindled; the renewed eruption of Mount St. Helens, 2004–2006*, U.S. Geological Survey Professional Paper 1750, 856 pp.

Temkin, S. (1981), *Elements of Acoustics*, Wiley and Sons. 515 pp.

Vergniolle, S., and Brandeis, G. (1994), *Origin of the sound generated by Strombolian explosions*, Geophys. Res. Lett. *21*, 1959-1962.

Vergniolle, S., and Brandeis, G. (1996), *Strombolian explosions: a large bubble breaking at the surface of a lava column as a source of sound*, J. Geophys. Res. *101*, 20433-20448.

Vergniolle, S., Brandeis, G., and Mareschal, J.C. (1996), *Strombolian explosions: Eruption dynamics determined from acoustic measurements*, J. Geophys. Res. *101*, 20449-20466.

Vergniolle, S., Boichu, M., and Caplan-Auerbach, J. (2004), *Acoustic measurements of the 1999 basaltic eruption of Shishaldin volcano, Alaska: 1) Origin of Strombolian activity*, J. Volcanol. Geotherm. Res. *137*, 109-134.

Vergniolle, S., and Caplan-Auerbach, J. (2004), *Acoustic measurements of the 1999 basaltic eruption of Shishaldin volcano, Alaska: 2) Precursor to the Subplinian activity*, J. Volcanol. Geotherm. Res. *137*, 135-151.

Vergniolle, S., and Ripepe, M. (2008), *From Strombolian explosions to fire fountains at Etna Volcano (Italy): what do we learn from acoustic measurements?* Geol. Soc., London, Special Publications *307*, 103-124.

Weill, A., Brandeis, G., Vergniolle, S., Baudin, F., Bilbille, J., Fevre, J.F., Pirron, B., and Hill, X. (1992), *Acoustic sounder measurements of the vertical velocity of volcanic jets at Stromboli volcano*, Geophys. Res. Lett. *19*, 2357-2360.

Withers, M., Aster, R., Young, C., Beiriger, J., Harris, M., Moore, S., and Trujillo, J. (1998), *A comparison of select trigger algorithms for automated global seismic phase and event detection*, Bull. Seism. Soc. Am. *88*, 95-106.

Figure captions

Fig. 1. Map of the summit area of Mt. Etna with the location of the five infrasonic sensors (triangles), composing the permanent infrasound network, and the eruptive fissure opened on May 13, 2008 (black line “EF”). The digital elevation model in the upper left corner shows the distribution of the four summit craters (VOR=Voragine, BN=Bocca Nuova, SEC=South-East Crater, NEC=North-East Crater).

Fig. 2. Infrasonic events recorded by EBEL station and corresponding spectra. The grey areas in (a,b,c) show the signal windows used to calculate the spectra. In particular, the events (a), (b) and (c) were generated at NEC, SEC and at the lowermost tip of EF, respectively.

Fig. 3. Scheme of the infrasound monitoring system (see text for details).

Fig. 4. Histogram showing the daily number of infrasonic events from August 1 to September 10, 2007, detected at EBEL station. The light grey rectangle indicates the period characterised by explosive activity at SEC.

Fig. 5. (a) Scheme of the volcanic activity of Mt. Etna at SEC, NEC and EF during January-June 2008 (1: explosive activity; 2: effusive activity; 3: degassing and/or deep explosive activity with no ash emission). **(b)** Peak-to-peak amplitude, **(c)** frequency, **(d)** quality factor and **(e,f)** source location of about 450 infrasonic events recorded during January-June 2008. The error bar in (e,f), calculated by using the method explained in **section 2.4**, was multiplied by a factor of 5 to become more visible. The volcanological information in (a) was provided by the internal reports of INGV (*http://www.ct.ingv.it/Etna2007/Main.htm*).

Fig. 6. (a,c,e) Examples of space distribution of semblance values calculated by locating three infrasonic events at Mt. Etna and (**b,d,f**) corresponding infrasonic signals at four different stations shifted by the time delay that allows obtaining the maximum semblance. The red squares and circles in (a,c,e) indicate four station sites and the nodes with the maximum semblance value, respectively. The black lines in (a,c,e) are the altitude contour lines from 3 to 3.3 km a.s.l..

Fig. 7. Digital elevation model of Mt. Etna summit with the source locations of the infrasound events, indicated by red circles, occurring during January-June 2008. The radii of the circles are proportional to the number of the locations in each grid node (see white circles and numbers reported in the lower right corner of the map). The sites of four infrasonic sensors are indicated with triangles.

Fig. 8. (a) Sketch of a vibrating bubble at the top of a magma column. R, L and h are, respectively, bubble radius and length, and thickness of the magma layer above the bubble (redrawn from Vergniolle et al., 2004). **(b)** The Helmholtz resonator is a rigid cavity of radius R and length L. Gas can escape through a small hole of radius R_{hole} with a velocity large enough to produce sound waves.

h is the thickness of magma layer above bubble (redrawn from Vergniolle and Caplan-Auerbach, 2004).

Fig. 9. The principle scheme for parameter estimation by Genetic Algorithm (GA). T_{comp} and T_{out} indicate the computational time and the fixed time-out, respectively.

Fig. 10. Comparison between the observed waveforms of infrasonic events recorded by EBEL station (red) and the synthetic ones (blue) considering Strombolian bubble vibration **(a)** and Helmholtz resonator **(b)** models. In (b) the bubble radius was fixed to 6 m. The observed waveform in (b) was low-pass filtered below 1.5 Hz, in order to remove harmonics.

Appendix A

Three source models of infrasound signals are applied in the proposed system: resonance of fluids in a conduit (Buckingham and Garces, 1996; Garces and McNutt, 1997; Hagerty et al., 2000), Strombolian bubble vibration (Vergniolle and Brandeis, 1994, 1996; Vergniolle et al., 1996, 2004; Vergniolle and Ripepe, 2008) and local coalescence within a foam (Vergniolle and Caplan-Auerbach, 2004).

A1. Resonating conduit

A pipe-like conduit, if affected by trigger mechanisms such as explosive processes, can resonate generating seismic and infrasonic signals. Both these signals are characterized by spectra with a fundamental mode and harmonics. The spectral content depends on conduit geometrical-chemical-physical features. The first characteristic influencing the frequency content of the radiated waves is the conduit length (L). The longer the conduit, the lower the frequency content. Moreover, also specific boundary conditions influence the resonating system. In fact, if the conduit is an open–open or closed–closed system has $n\lambda/2$ (λ = wavelength, n = 1,2,3,...) waves as longitudinal resonance modes whereas a system with one open and one closed end has $(2n-1)\ \lambda/4$ waves. Therefore, open–open or closed–closed systems produce signals with spectra characterized by evenly spaced peaks consisting of the fundamental mode, f_0, and a set of n integer harmonics which are multiples of f_0 (f_0, $f1 = 2\, f_0, f_2 = 3\, f_0, \ldots, f_n = n\, f_0$); on the other hand spectra that have equally spaced peaks and contain only odd harmonics ($f_0, f_1 = 3f_0, f_2 = 5f_0, \ldots, f_n = (2n-1)\, f_0$) are linked to resonant systems with one open and one closed end (De Angelis and McNutt, 2007). Finally, the frequency is also directly related to the wave velocity of the fluid in the conduit (c). The fluid could be gas or bubbly magma with a very wide range of variability of velocity. If air or pure hot gas are considered, their wave velocity are equal to 0.34 and 0.704 km/s (Weill et al., 1992), respectively. If we take into account bubbly magma, the wave velocity ranges from 0.3 km/s (Aki et al. 1977) to 2.5 km/s (Murase and McBirney, 1973), according to different flow conditions and magma properties (above all the gas fraction). Considering these prospective fluids filling the conduit, the lower end of the resonating system can consist in the interface between bubbly-magma or gas and non-vesciculated magma. Because of the strong impedance contrast between the source fluid and the underlying non-vesciculated magma, this termination acts like a closed termination (De Angelis and McNutt, 2007). The upper end of the conduit can be either open to the atmosphere and act as an open termination, or obstructed by a relatively viscous plug at the vent acting as a closed boundary. In any case, the observation that the conduit is plugged at the vent (e.g. high porosity materials) does not necessarily imply that it is an acoustically closed boundary (Garces and McNutt, 1997).

In the light of these parameters, the fundamental mode of the generated signal is equal to (Hagerty et al., 2000):

$$f_0 = \frac{c}{2L} \tag{A1}$$

A2. Strombolian bubble vibration

In the Strombolian bubble vibration model the infrasound is produced by the vibration of a thin layer of magma, pushed by a variation of pressure inside a shallow metric bubble prior bursting. The bubble shape is approximated by a hemispherical head and a cylindrical tail, as expected in slug-flow (**Fig. 8a**). The radius of the bubble R varies around its equilibrium radius R_{eq} by (Vergniolle and Brandeis, 1996):

$$R = R_{eq}(1+\varepsilon) \tag{A2}$$

where ε is the dimensionless radius of the bubble. The bubble volume V_g can be calculated by (Vergniolle and Brandeis, 1996):

$$V_g = \frac{2\pi R^3}{3} + \pi R_0^2 L \tag{A3}$$

where L is the bubble length, R_0 is the initial radius. R_{eq} can be obtained by the following adiabatic law (Vergniolle and Brandeis, 1996):

$$R_{eq} = \left\{ \frac{3R_0^2}{2} \left[\left(\frac{2R_0}{3} + L \right) \left(1 + \frac{\Delta P}{p_{air}} \right)^{\frac{1}{\gamma}} - L \right] \right\}^{\frac{1}{3}} \tag{A4}$$

where ΔP is the initial overpressure, p_{air} is the air pressure, γ is the ratio of specific heats. The Strombolian bubble vibration model is based on the general equation for the bubble vibration (Vergniolle and Brandeis, 1996):

$$\ddot{\varepsilon} + \left(\frac{12\mu}{\rho_l R_{eq}^2}\right)\dot{\varepsilon} + \frac{p_{air}\left[1-\left(\frac{V_{eq}}{V_g}\right)^{\gamma}\right]}{\rho_l R_{eq} h}(1+\varepsilon)^2 = 0 \tag{A5}$$

where μ is the viscosity, ρ_l is the magma density, V_{eq} is the equilibrium value of the gas volume, h is the thickness of the thin upper membrane. It is worth noting that V_g is a function of ε. The first initial condition to be specified is the initial value of the dimensionless radius ε_0. The second initial condition is the initial radial acceleration $\ddot{\varepsilon}_0$, which depends on the initial force applied to the layer of magma. Assuming that the bubble, at rest at the magma-air interface is suddenly overpressurized by an amount ΔP, this force is directly related to the bubble overpressure. Therefore the initial conditions are (Vergniolle and Brandeis, 1996):

$$\ddot{\varepsilon}_0 = \frac{\Delta P R_0^2}{\rho_l R_{eq}^3 h_{eq}} \tag{A6}$$

$$\varepsilon_0 = \frac{R_0}{R_{eq}} - 1 \tag{A7}$$

Ignoring viscous damping and assuming small oscillations our equation has only one physically possible solution, which is a simple oscillator. Therefore, on the basis of these assumptions the excess pressure in air is expressed as a sinusoidal function:

$$p_{ac} - p_{air} = -\rho_{air} R_{eq}^3 \frac{A\omega^2}{r}\sin(\omega t + \phi) \tag{A8}$$

where the amplitude A, the radian frequency ω and the phase delay φ are:

$$A = \frac{\Delta P R_0^2}{3\gamma p_{air} R_{eq}^2}\left(\frac{2 + 3L/R_{eq}}{2}\right) \tag{A9}$$

$$\omega = \left[\frac{3\gamma p_{ext}}{\rho_l R_{eq} h_{eq}}\left(\frac{2}{2 + 3L/R_{eq}}\right)\right]^{1/2} \tag{A10}$$

$$\phi = -\frac{\pi}{2} \tag{A11}$$

where p_{ext} is close to the atmospheric pressure p_{air}. In general, the **equation (A5)** has no analytical solution. We solved it by numerical integration (a fourth order Runge-Kutta method). Finally, in order to calculate the excess pressure in air, the following equation is used (Vergniolle and Brandeis, 1996):

$$p_{ac} - p_{air} = \left[2\dot{R}^2\left(t - r/c\right) + R\left(t - r/c\right)\ddot{R}\left(t - r/c\right)\right]\frac{\rho_{air} R\left(t - r/c\right)}{r} \tag{A12}$$

where t is time, r is the distance source-sensor and c is the speed of sound in air, 340 m/s (Lighthill, 1978).

A3. Helmholtz resonator

For a piston emitting sound in a halfspace, acoustic pressure is (Vergniolle and Caplan-Auerbach, 2004):

$$p_{ac} - p_{air} = \frac{\rho_{air}\ddot{\xi}R_{hole}^2}{2\pi r} \tag{A13}$$

where ξ is the displacement of air, R_{hole} is the hole radius. If the dimensions of the resonator are small compared to the wavelength, the behavior of an element of air in the neck of an undriven Helmholtz resonator is (Vergniolle and Caplan-Auerbach, 2004):

$$m_{helm}\ddot{\xi} + R_{helm}\dot{\xi} + s_{helm}\xi = 0 \tag{A14}$$

where m_{helm}, R_{helm} and s_{helm} are the mass, the resistance coefficient leading to damping and the stiffness coefficient of the oscillator, respectively (Vergniolle and Caplan-Auerbach, 2004):

$$m_{helm} = \rho_{air}\varepsilon S_{hole} \tag{A15}$$

$$R_{helm} = \frac{\rho_{air}\omega^2 S_{hole}^2}{2\pi c} \tag{A16}$$

$$s_{helm} = \frac{\rho_{air}c^2 S_{hole}^2}{V_{helm}} \tag{A17}$$

where ρ_{air} is the air density, S_{hole} is the hole area, V_{helm} is the volume of the resonator, ε is the effective length of the orifice (calculated as $\varepsilon = 8R_{hole}/3\pi$; Temkin, 1981). S_{hole} and V_{helm} are calculated as follows (Vergniolle and Caplan-Auerbach, 2004):

$$S_{hole} = \pi R_{hole}^2 \quad \text{(A18)}$$

$$V_{helm} = \pi R^2 L + 2\pi R^3 / 3 \quad \text{(A19)}$$

where R and L are radius and length of the bubble, respectively. The air acceleration $\ddot{\xi}$ can be calculated by (Vergniolle and Caplan-Auerbach, 2004):

$$\ddot{\xi} = -\omega^2 A \exp(-t/\tau)\cos(\omega t + \varphi) \quad \text{(A20)}$$

where ω and τ, radian frequency and relaxation time, respectively, are:

$$\omega = c\left(S_{hole} / \varepsilon V_{helm}\right)^{1/2} \quad \text{(A21)}$$

$$\tau = \frac{2m_{helm}}{R_{helm}} \quad \text{(A22)}$$

and, finally, A and φ are arbitrary constants for a damped harmonic solution and are calculated as follows:

$$A = -\frac{\Delta P}{\rho_{air} \varepsilon \omega^2 \cos\varphi} \quad \text{(A23)}$$

$$\varphi = \arctan\left[\frac{-1}{\omega\tau}\right] \quad \text{(A24)}$$

These equations of the Helmholtz resonator are not able to model harmonics, but only the fundamental mode of vibration.

Figures

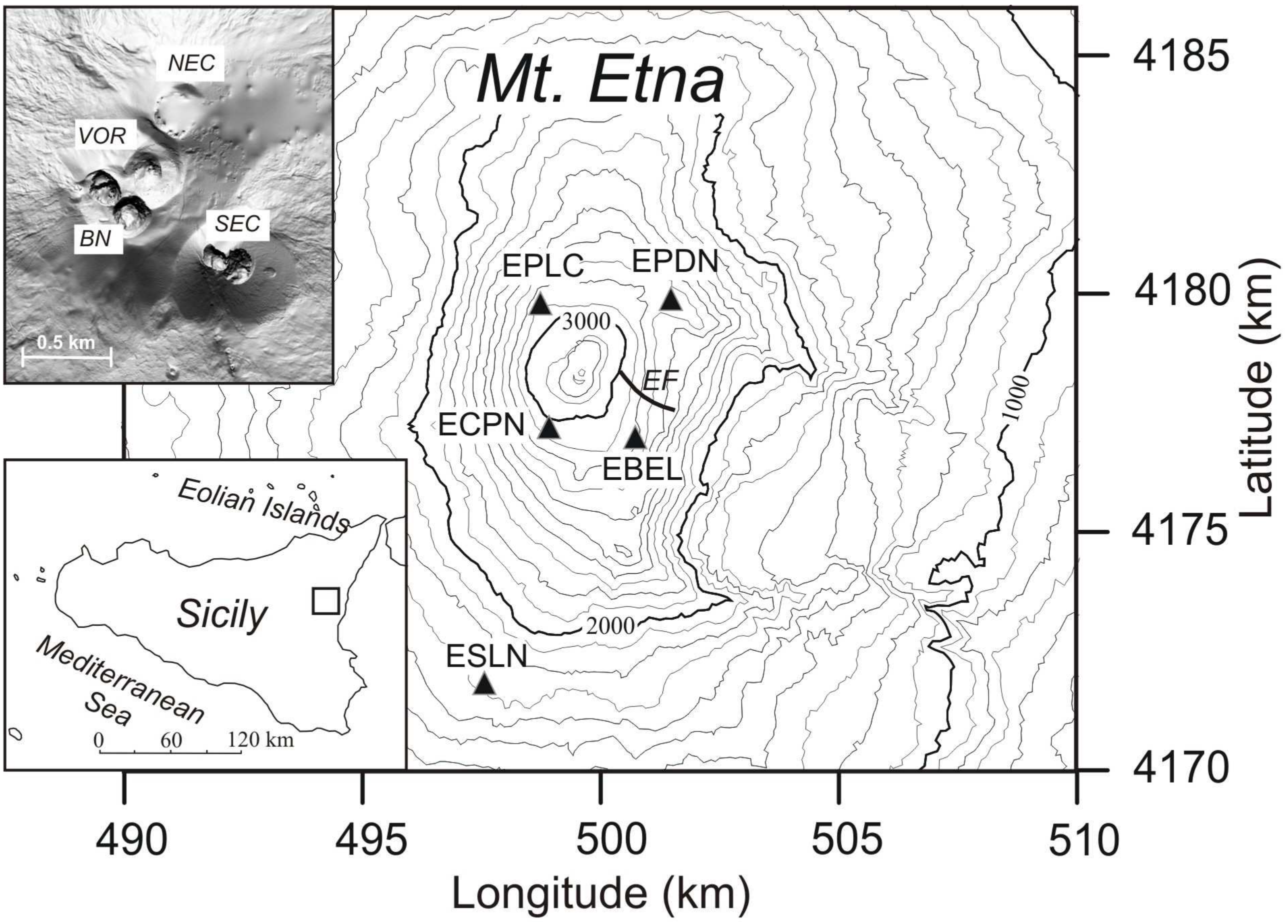

Fig. 1

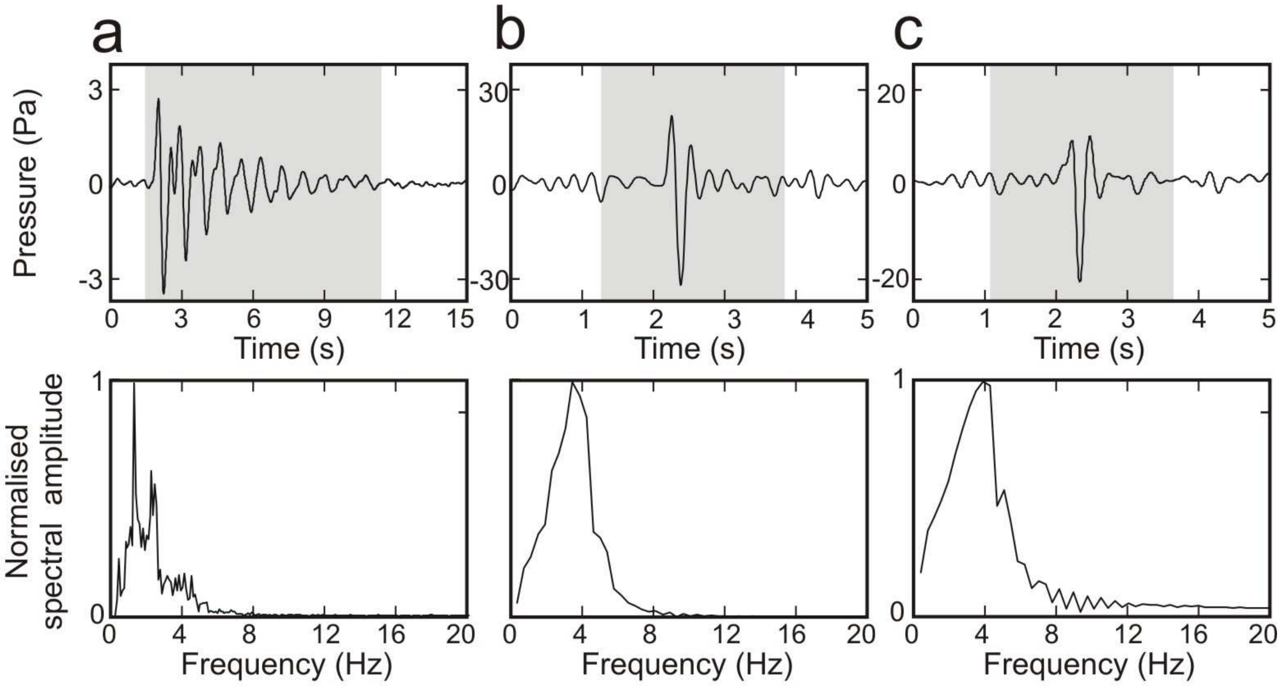
a
b
c
Pressure (Pa)
3
0
-3
30
0
-30
20
0
-20
0
3
6
9
12
15
0
1
2
3
4
5
Time (s)
Normalised spectral amplitude
1
0
4
8
12
16
20
Frequency (Hz)

770

771 **Fig. 2**

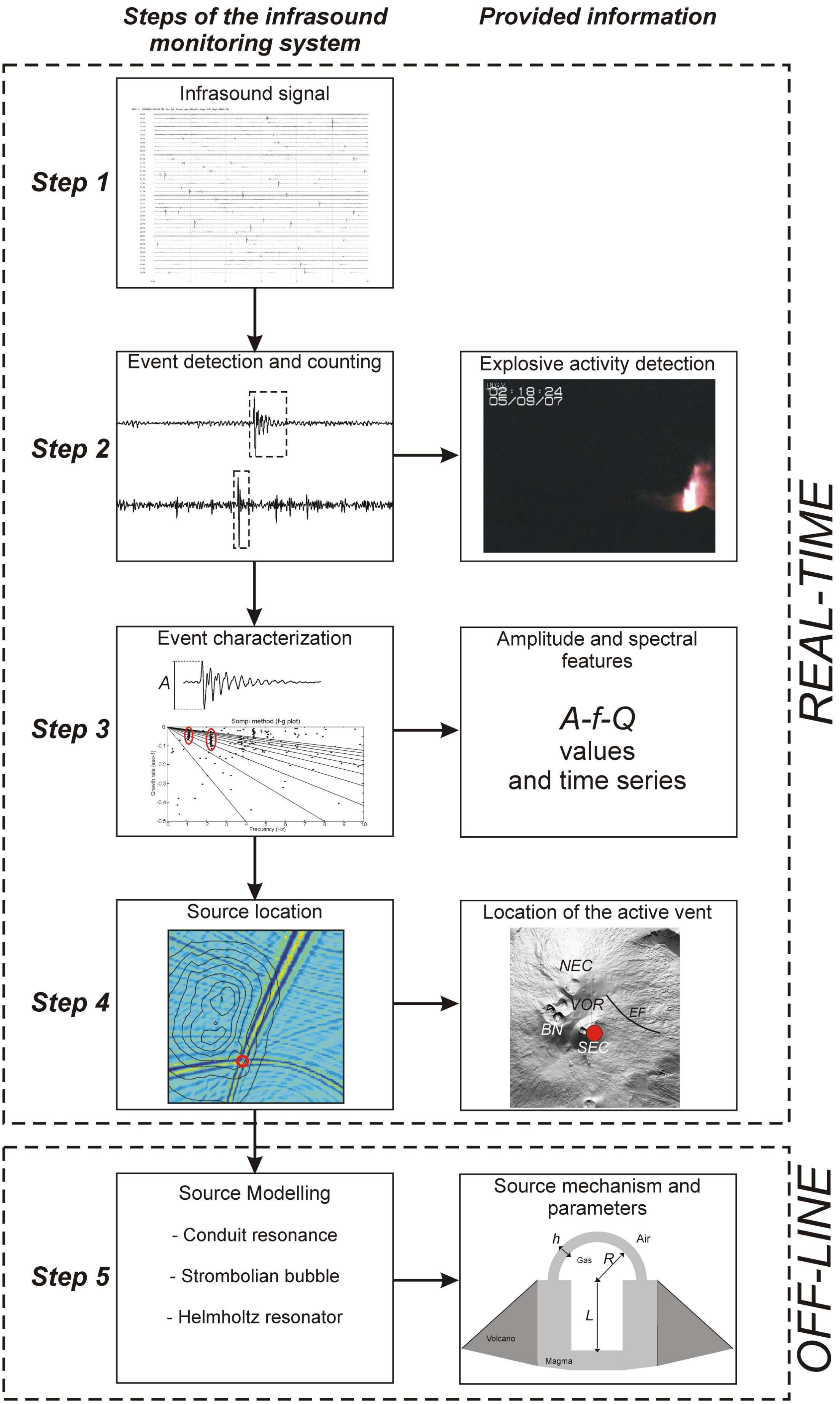
Steps of the infrasound monitoring system
Provided information
Infrasound signal
Step 1
Event detection and counting
Step 2
Explosive activity detection
02:18:24
05/09/07
Event characterization
Step 3
A
Sompi method (f-g plot)
Frequency (Hz)
Amplitude and spectral features
A-f-Q
values
and time series
REAL-TIME
Source location
Step 4
Location of the active vent
NEC
VOR
EF
BN
SEC
Source Modelling
Step 5
- Conduit resonance
- Strombolian bubble
- Helmholtz resonator
Source mechanism and parameters
h
Air
Gas
R
L
Volcano
Magma
OFF-LINE

Fig. 3

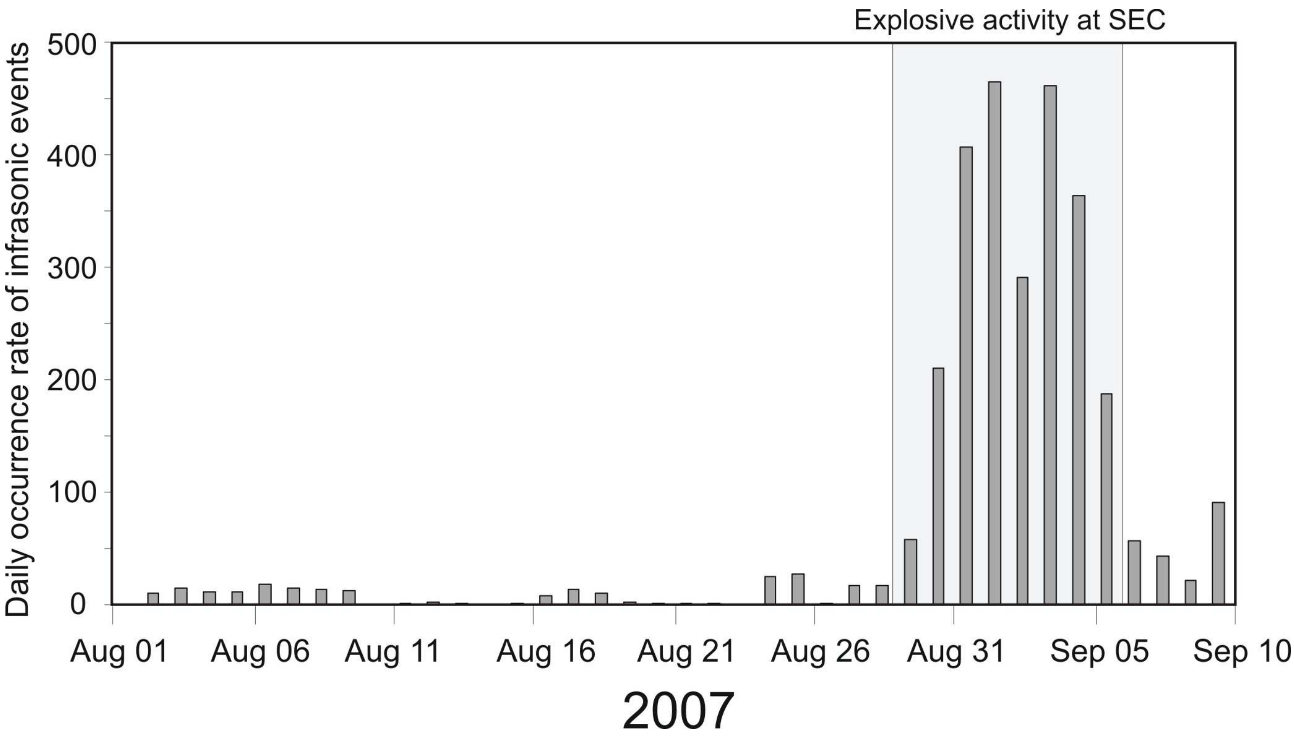
Explosive activity at SEC
Daily occurrence rate of infrasonic events
500
400
300
200
100
0
Aug 01
Aug 06
Aug 11
Aug 16
Aug 21
Aug 26
Aug 31
Sep 05
Sep 10
2007

Fig. 4

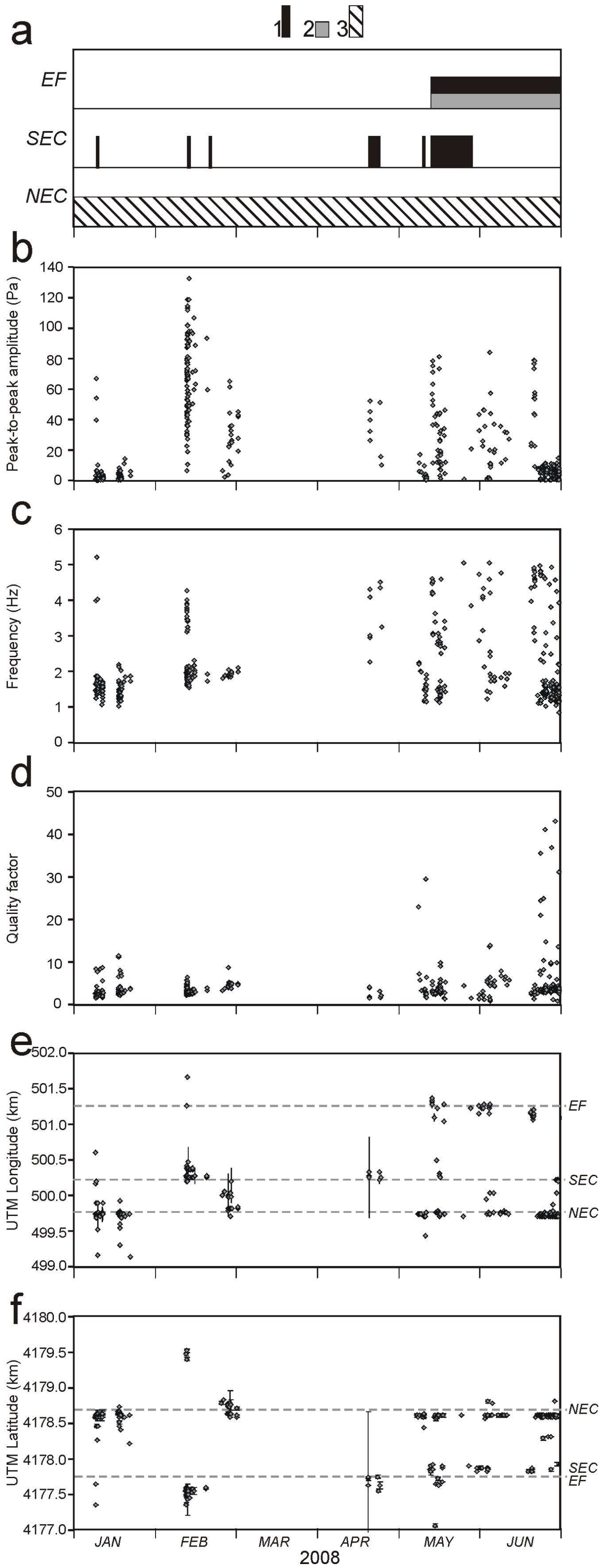
a
1
2
3
EF
SEC
NEC
b
Peak-to-peak amplitude (Pa)
c
Frequency (Hz)
d
Quality factor
e
UTM Longitude (km)
EF
SEC
NEC
f
UTM Latitude (km)
NEC
SEC
EF
JAN
FEB
MAR
APR
MAY
JUN
2008

776
777 **Fig. 5**

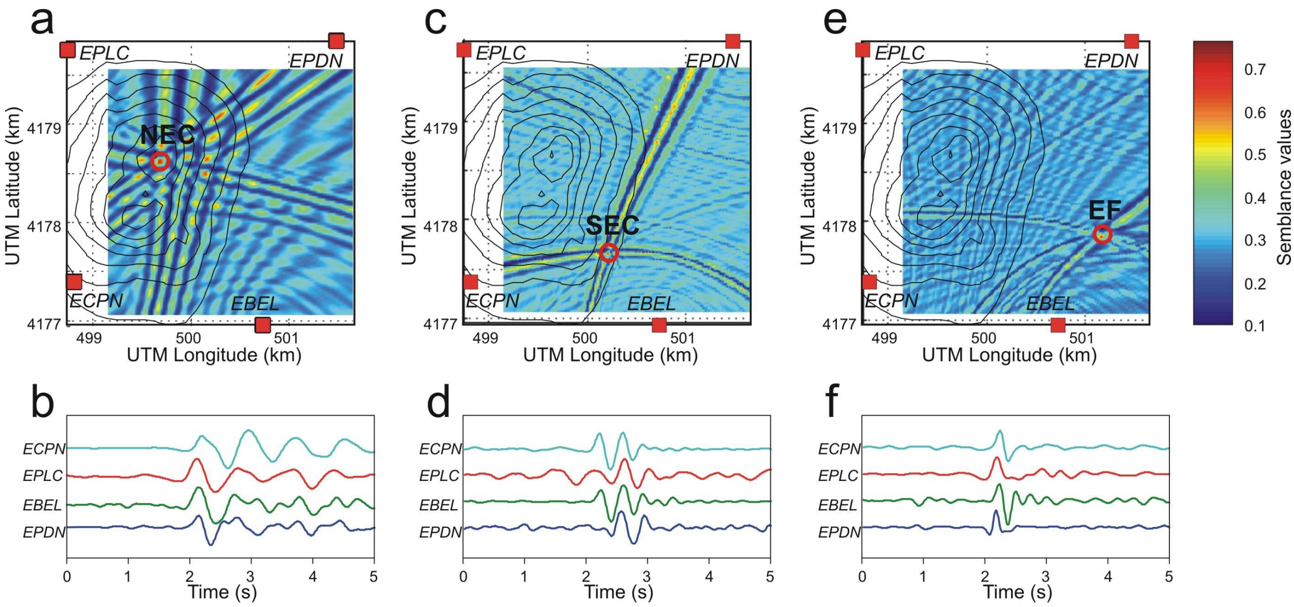

a
EPLC
EPDN
NEC
ECPN
EBEL
UTM Latitude (km)
UTM Longitude (km)
c
SEC
e
EF
Semblance values
b
d
f
ECPN
EPLC
EBEL
EPDN
Time (s)

778

779 **Fig. 6**

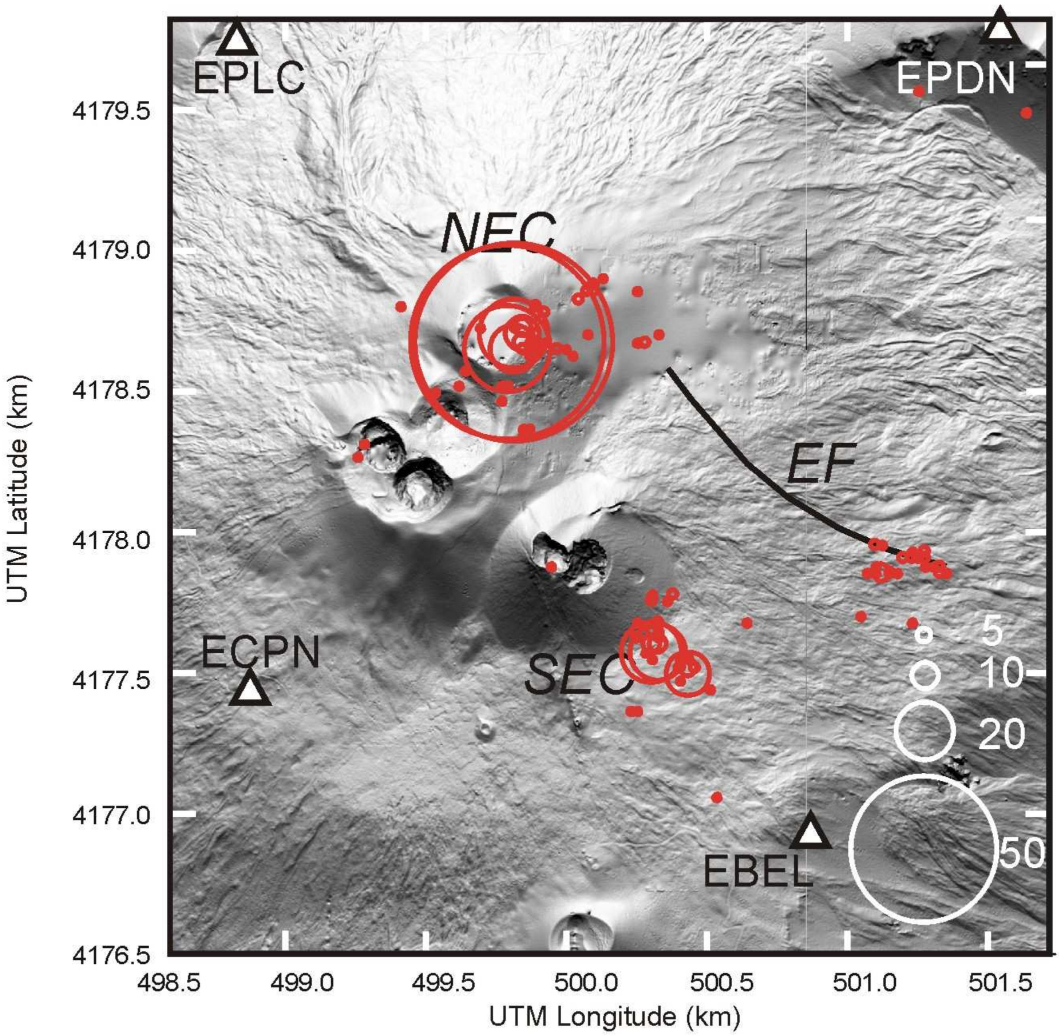
EPLC
EPDN
NEC
EF
SEC
ECPN
EBEL
5
10
20
50
4179.5
4179.0
4178.5
4178.0
4177.5
4177.0
4176.5
UTM Latitude (km)
498.5
499.0
499.5
500.0
500.5
501.0
501.5
UTM Longitude (km)

780

781 **Fig. 7**

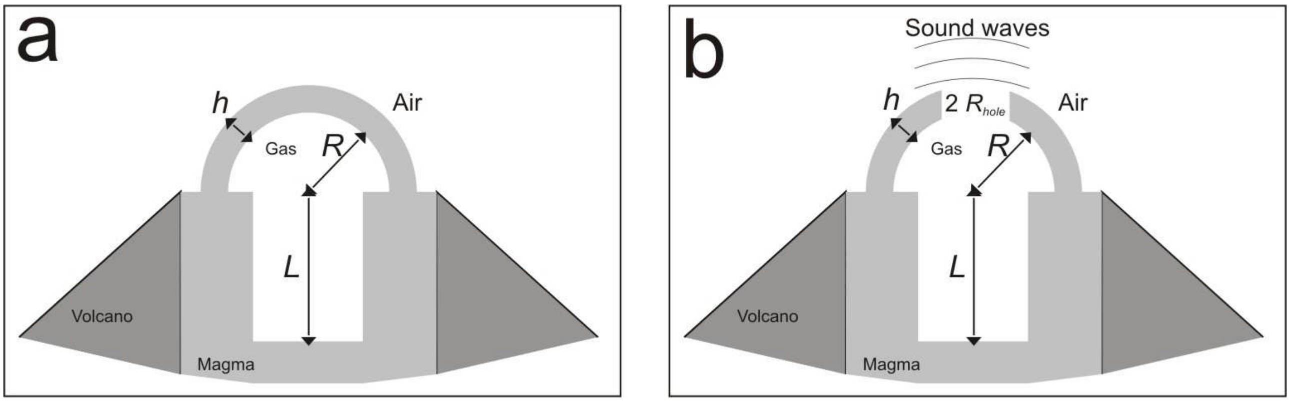

a
h
Air
Gas
R
L
Volcano
Magma
b
Sound waves
h
2 R_hole
Air
Gas
R
L
Volcano
Magma

Fig. 8

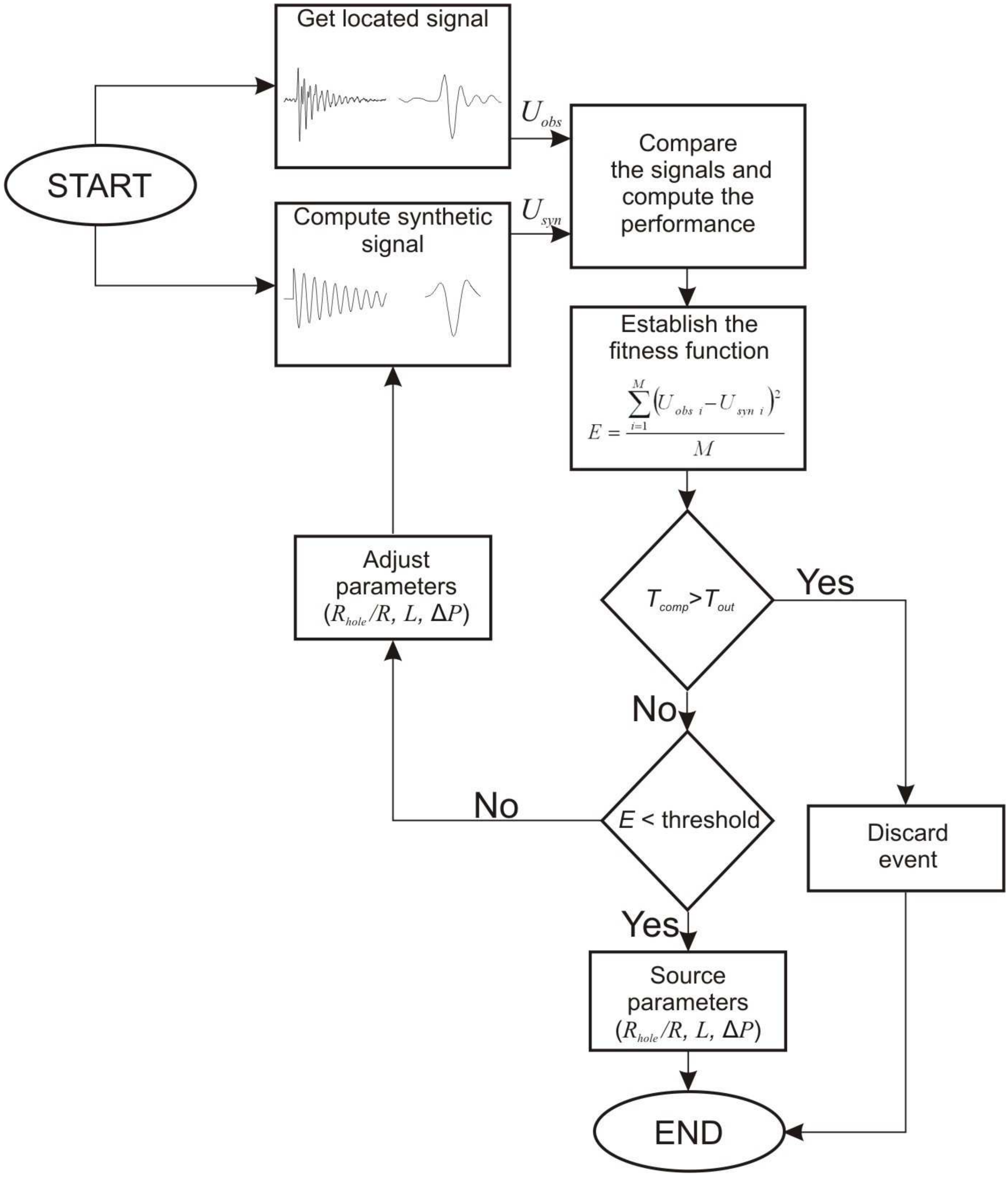

Get located signal
START
Compute synthetic signal
U_{obs}
U_{syn}
Compare the signals and compute the performance
Establish the fitness function
$E = \frac{\sum_{i=1}^{M} (U_{obs\ i} - U_{syn\ i})^2}{M}$
Adjust parameters (R_{hole}/R, L, ΔP)
$T_{comp} > T_{out}$
Yes
No
No
E < threshold
Discard event
Yes
Source parameters (R_{hole}/R, L, ΔP)
END

784

785 **Fig. 9**

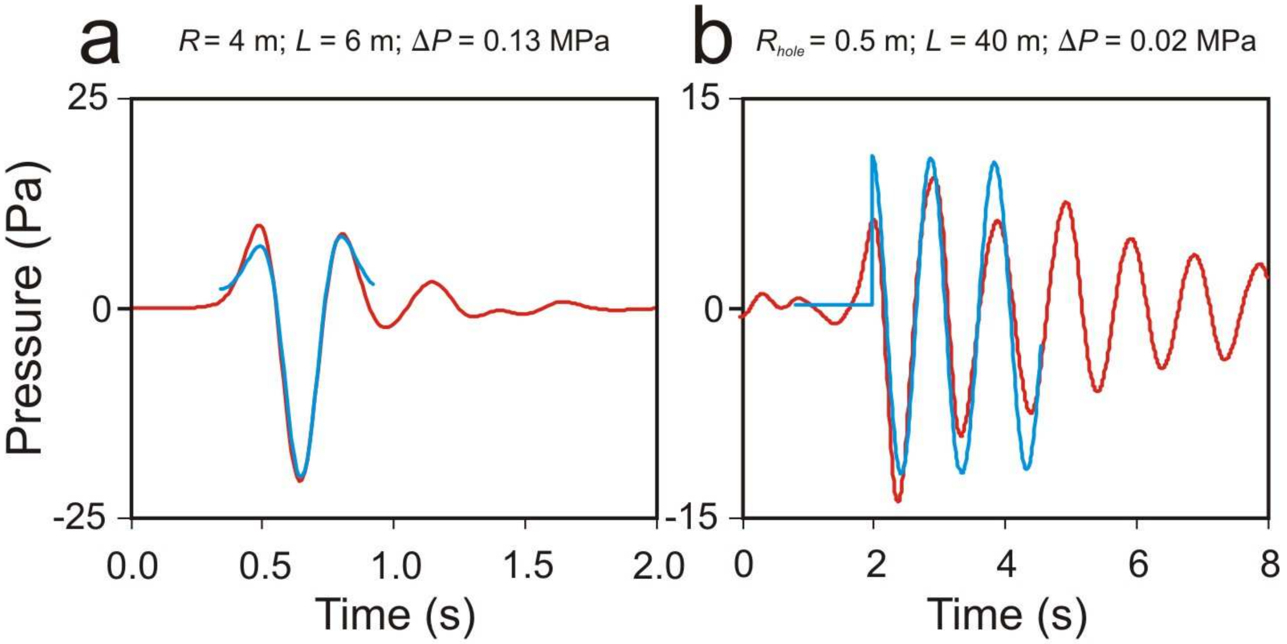
a
R = 4 m; L = 6 m; ΔP = 0.13 MPa
b
R_hole = 0.5 m; L = 40 m; ΔP = 0.02 MPa
Pressure (Pa)
25
0
-25
15
0
-15
0.0
0.5
1.0
1.5
2.0
0
2
4
6
8
Time (s)
Time (s)

Fig. 10